Applied Catalysis B: Environmental 304 (2022) 120983

Contents lists available at ScienceDirect

Applied Catalysis B: Environmental

journal homepage: www.elsevier.com/locate/apcatb

Carbon dots enhance the interface electron transfer and photoelectrochemical kinetics in TiO_2 photoanode

Yidong Han [a], Jie Wu [a], Yi Li [a], Xiaoqing Gu [a], Tiwei He [a], Yu Zhao [b,*], Hui Huang [a,*], Yang Liu [a,*], Zhenhui Kang [a,c,**]

[a] Institute of Functional Nano & Soft Materials (FUNSOM), Jiangsu Key Laboratory for Carbon-Based Functional Materials & Devices, Soochow University, 199 Ren'ai Road, Suzhou 215123, Jiangsu, China
[b] Department of Information Technology, Suzhou Institute of Trade & Commerce, 287 Xuefu Road, Suzhou 215009, Jiangsu, China
[c] Macao Institute of Materials Science and Engineering, Macau University of Science and Technology, Taipa 999078, Macau SAR, China

ARTICLE INFO

Keywords:
TiO_2 photoanode
Nitrogen-doped carbon dots
Photoelectrochemical activities
In-situ transient photovoltage

ABSTRACT

Photoelectrochemical (PEC) water splitting is one of the most promising strategies to turn solar energy into chemical fuels. The low efficiency of photo-generated charge separation caused by fast electron-hole recombination is regarded as a challenge that hinders the further improvement of TiO_2 photoanode performance in PEC cells. Here, the nitrogen-doped carbon dots (N-CDs) anchored TiO_2 photoanodes were fabricated by one-step hydrothermal method. The in-situ transient photovoltage (TPV) technology shows that electron-trap effect is formed in TiO_2 photoanode due to the existence of N-CDs. Meanwhile, the enhancement of photo-generated charge separation efficiency was proven as the charge extraction of TiO_2 is promoted by ~160% after anchoring N-CDs. Besides, N-CDs increase the conductivity of TiO_2 photoanode and promote the efficiency of photo-generated charge transfer. In addition, the impedance of TiO_2 photoanode and its interface are reduced by ~ 34% and ~ 66%, respectively. Under AM 1.5G light intensity and 1.23 V vs. RHE, the highest photocurrent densities of TiO_2/N-CDs (TNCD-15 mg) is 3.09 mA cm^{-2} in 1.0 M NaOH, which is ~ 3.22 times as high as that of the primitive TiO_2. This work explains the mechanism of anchoring N-CDs to improve PEC performance through in-situ characterization, which provides a new idea for PEC material design to achieve higher PEC performances.

1. Introduction

Artificial photosynthesis system, which can efficiently and economically convert solar energy into chemical fuels in accordance with global energy needs, is an important strategy to achieve a sustainable carbon neutral society [1–3]. In this system, photoelectrochemical (PEC) water splitting has been regarded as a reasonable method, which converts solar energy to hydrogen energy with high energy density [4–6]. As an essential part, various semiconductor photoelectrode, such as WO_3 [7,8], Fe_2O_3 [9,10], $BiVO_4$ [11,12] and Cu_2O [13,14] are broadly used to promote PEC water splitting. Among them, TiO_2 is considered to be the most representative photoelectrode for exploring PEC water splitting owing to its suitable band-edge position, ability to bear light corrosion, natural rich, non-toxic and low cost [15,16]. However, due to fast electron-hole recombination and relatively large band gaps, the theoretical applied bias photon to current efficiency (ABPE) efficiency of TiO_2 photoanode is ca. 2% even if the light absorption efficiency of TiO_2 is 100% and all converted into hydrogen energy [17–19]. Thus, some modifications have been carried out to promote the ABPE of TiO_2 photoanode, which includes but not limited to non-metallic doping of C/N [20,21] which adjusts the position of the valence band and increase the carrier density; metal doping of Fe/Ni/Co/Sn [22–25] which enhance light absorption and increase charge transfer rate; self-doping of Ti^{3+} [26] which reduces charge recombination rate, narrows down band gap, introduces oxygen vacancies as well as promotes charge separation and transfer.

Recently, quantum dots modified TiO_2 has aroused great interest due to the excellent photoelectric properties and multiple exciton generation possibilities of semiconductor quantum dots [27,28]. Sun et al. deposited CdS quantum dots into TiO_2 nanotube through a sequential

* Corresponding authors.
** Corresponding author at: Institute of Functional Nano & Soft Materials (FUNSOM), Jiangsu Key Laboratory for Carbon-Based Functional Materials & Devices, Soochow University, 199 Ren'ai Road, Suzhou 215123, Jiangsu, China.
E-mail addresses: 2021022101@szjm.edu.cn (Y. Zhao), hhuang0618@suda.edu.cn (H. Huang), yangl@suda.edu.cn (Y. Liu), zhkang@suda.edu.cn (Z. Kang).

https://doi.org/10.1016/j.apcatb.2021.120983
Received 24 July 2021; Received in revised form 11 November 2021; Accepted 28 November 2021
Available online 3 December 2021

chemical bath deposition (S-CBD) method and the CdS modified TiO_2 photoanode can reach a significant PEC performance in 1.0 M Na_2S solution at 138.4 mW/cm^2 illumination (AM 1.5 G) [29]. However, protective layer such as amorphous TiO_2 and PEDOT are essential for CdS modified photoanodes due to the production of Cd^{2+} by light corrosion of CdS. Therefore, a more objective quantum dot is urgently needed to modify TiO_2 photoanodes. Carbon dots (CDs) are considered as an alternative quantum dots due to their excellent optical and electric properties in the field of PEC, such as great electron storage property, photo-generated carries transfer medium and large specific surface area [30,31]. Bian et al. explored the influence of CDs amount on PEC performance and deeply analyzed the relationship between photocurrent density and impedance, finding that the addition of CDs can reduce the interface impedance between the photoanode and the electrolyte [32]. Luo et al. reported that loading N-CDs on TiO_2 nanoparticle to promote the PEC activity of TiO_2, which can reach a maximum photocurrent density of 0.15 mA cm^{-2} at 0.3 V vs. RHE, and the synergistic effect of N-CDs combined with TiO_2 was found through photoluminescence (PL) [33]. Liang et al. used the dipping method to load the CDs on the hydrogen-treated TiO_2, the photoanode can reach a photocurrent density of 3.0 mA cm^{-2} at 1.23 V vs. RHE due to the formation of oxygen vacancies and the enhancement of light absorption by carbon dots [34]. However, the effect of CDs on the charge transport kinetics of TiO_2 photoanodes has rarely been visually characterized and studied, which has become an obstacle to further improve PEC performance.

In this work, N-CDs anchored TiO_2 photoanodes were synthesized by the one-step hydrothermal method. With in-situ transient photovoltage (TPV), we show that N-CDs can trap the photo-generated electron from TiO_2, which improves the efficiency of photo-generated charge generation. Meanwhile, the N-CDs increasing the conductivity of TiO_2 photoanode as well as the charge separation and transfer efficiency are confirmed. Comparing the quantified performance of N-CDs anchored TiO_2 with primitive TiO_2, the maximum amount of photo-generated charge is promoted by ~ 160%; the charge transfer rate is promoted

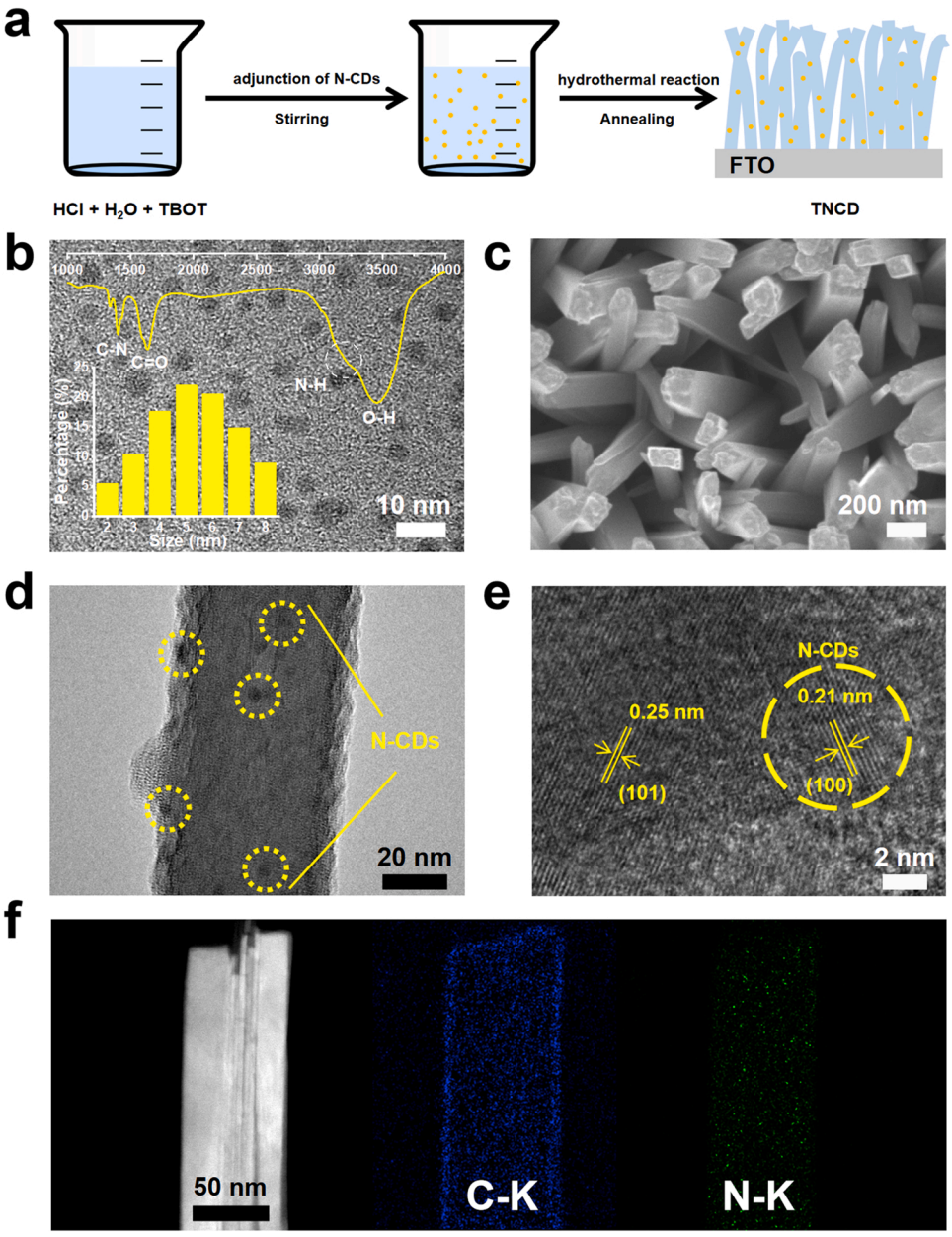

Fig. 1. (a) Synthetic diagram of TNCD, (b) the FT-IR spectrum and distribution map of N-CDs, (c) SEM image, (d) TEM image, (e) HRTEM image of TNCD, and (f) elemental mapping images of TNCD-15 mg.

by ~ 428%; the carrier density is promoted by ~ 913% and the impedance of photoanode as well as its interface are reduced ~ 34% and ~ 66%, respectively. Under AM 1.5 G light intensity and 1.23 V vs. RHE, the highest photocurrent densities of TNCD-15 mg is 3.09 mA cm^{-2} in 1.0 M NaOH, which is ~ 3.22 times of that of the primitive TiO_2 photoanode.

2. Experimental

2.1. Preparation of N-CDs

Firstly, the primitive CDs were synthesized by using typical electrochemical methods. Briefly, two graphite rods are placed in 1.0 L deionized water as electrodes, and 30 V DC power supply is applied for the electrolysis. After 20 days of continuous electrolysis, a dark brown CDs solution was obtained. For N-CDs fabrication, 15 mL ammonia (28%) and 15 mL concentrated CDs solution (0.2 mg/mL) were put into autoclave and kept at 150 °C for 6 h. After that, the resulting N-CDs solution was filtered before it can be used.

2.2. Synthesis of primitive TiO_2 and N-CDs anchored TiO_2 photoanodes

As shown in Fig. 1a. Firstly, 30 mL deionized water was added into 30 mL hydrochloric acid solution and stirred for 10 min. Secondly, 1 mL tetrabutyl titanate (TBOT) solution was added and stirred for 20 min. Finally, added a certain quality of N-CDs and stirred for 20 min. The solution temperature is room temperature after stirring.

After completing the above operations, pour 10 mL as-prepared precursor solution into 50 mL PTFE liner. Put the FTO conductive surface down into the PTFE liner, seal and heat it at 150 °C for 8 h in an oven. Previously, FTO conductive glass was ultrasonically cleaned with professional cleaning agent, acetone, ethanol, and deionized water for 30 min each. After heating for 8 h, take out the conductive glass, rinse with deionized water, dry at 70 °C for 30 min, and roast at 550 °C for 3 h in a muffle furnace. Different sample names and the corresponding quality of N-CDs are shown in the Table S1. Primitive TiO_2 photoanodes were synthesized by the above method without adding N-CDs.

3. Results and discussion

3.1. Characterization of photoanode

The morphologies of the modified TiO_2 and N-CDs had been characterized via scanning electron microscope (SEM) as well as transmission electron microscope (TEM). The N-CDs distribution map is shown in Fig. 1b, which suggests the as-prepared N-CDs with the dimensions of 2–8 nm in a massive proportion. After standing for six months, the size distribution of N-CDs remains basically unchanged, indicating that N-CDs can exist stably without agglomeration or decomposition (Fig. S1) [35]. The surface functional groups composition and surface state of N-CDs were analyzed by Fourier transform infrared spectroscopy (the inset of Fig. 1b), where the peaks located at 1400 and 1635 cm^{-1} are considered to C-N and C═O, and the two peaks located at 3200 and 3454 cm^{-1} mean the O—H and N—H bond stretching vibrations, respectively. The FT-IR spectrum of N-CDs illustrates that N-CDs have abundant carboxyl, hydroxyl, and amino functional groups [36]. Fig. 1c is the SEM image of TNCD-15 mg, which shows an identical morphology of nanorods as formerly reported. Compared with primitive TiO_2 (Fig. S2a), the nanorods of TNCD-15 mg are extra regular in diameter. Besides, as the quality of N-CDs increases, the diameter of the nanorods gradually decreases (Fig. S2b-S2d). Besides, as the quality of N-CDs increases, the diameter of the nanorods gradually decreases (Fig. S2b-S2d). The phenomenon can be inferred that the N-CDs have stronger adsorption to the {100} surfaces, which affects the growth of TiO_2 along the diameter direction and makes the nanorods finer. The finer TiO_2 nanorods lead to more surface area exposed to the solution and incident light, increasing the number of active sites of the modified photoanode and promoting the photoelectrochemical activity of the samples. The above suggests N-CDs can improve the performance of PEC by adjusting the morphology of photoanode [37]. The standard TEM image of TNCD-15 mg is shown in Fig. 1d, from which the N-CDs anchored in the nanorods of TiO_2 can be seen, and dimensions of N-CDs are maintained at 2–8 nm, indicating the stability of N-CDs in material manipulating is great [38]. Fig. 1e is the HRTEM image of TNCD-15 mg. The lattice spacing of 0.25 nm is known as the {101} facets of TiO_2 and the lattice spacing of 0.21 nm corresponds to the {100} planes of N-CDs [39]. Energy dispersive X-ray spectroscopy (EDS) analyzed from remote particles figures out numerous factors of TNCD-15 mg, particularly titanium, oxygen, carbon and nitrogen because they are the primary chemical elements (Fig. S3). Besides, the elemental mapping was conducted to identify that the N-CDs are anchored in TiO_2 and the consequences are shown in Fig. 1f. It can be confirmed that the N-CDs are existed in TiO_2 from the C and N elemental mapping.

X-ray diffraction (XRD) was utilized to study the effect of N-CDs on the growth of TiO_2 crystals. As shown in Fig. 2a, regardless of whether carbon dots are added, the peak positions are basically the same, which indicates that the as-prepared photoanodes mainly exposed {101} and {112} facets on the top surface of the photoelectrode. It is worth noting that TNCD-15 mg has higher peak intensities than that of TiO_2. This phenomenon can be attributed to the surface functional groups on N-CDs, which can be used as the nucleation center of TiO_2. After adding N-CDs, these groups will complex Ti^{4+} ions, which is conducive to the nucleation of TiO_2. Besides, {101} and {112} facets are corresponding to the thermodynamically stable facets and reactive facets [40], and the comparison of the FWHM clarified that the addition of N-CDs promoted a better crystallinity of {112} facets, which is beneficial to enhance the photoelectrochemical activity. Meanwhile, the ratio of {101}/{112} of TNCD-15 mg is 4.49, which is significantly larger than that of TiO_2 (Table S2). It has been clarified that the change of particle shape can be expressed by the relative intensity of two XRD peaks [41]. Therefore, although the addition of N-CDs maintains the main crystal structure of the TiO_2 nanorode, the crystal size and preferred orientation direction are slightly changed.

The Raman spectra of N-CDs, TiO_2, and TNCD-15 mg are shown in Fig. 2b. As shown in the spectrum of N-CDs, two obvious characteristic Raman peaks located at 1332 cm^{-1} and 1597 cm^{-1} are corresponded to the Raman-active D-band and G-band of N-CDs respectively. As for the Raman spectrum of TiO_2, the peaks belonged to E_g and A_{1g} mode are located at 446 cm^{-1} and 608 cm^{-1} respectively, and the peak centered at 236 cm^{-1} (marked as *) is attributed to a characteristic peak of rutile TiO_2, which is a compound vibration peak caused by multi-phonon scattering process [42]. Therefore, there are five peaks existed in the Raman spectra of TNCD-15 mg, indicating stable existence of N-CDs in TiO_2.

To understand the chemical states of modified TiO_2 photoanode, X-ray photoelectron spectroscopy (XPS) was carried out. Fig. S4 is the XPS Ti 2p spectrum. The curve of TiO_2 exists shoulder peaks at ca. 458.6 and 464.3 eV, which are considered to Ti $2p_{3/2}$ and Ti $2p_{1/2}$ for Ti^{4+} in TiO_2 [43,44]. Compared to the Ti 2p curve of TiO_2, the two peaks of TNCD-15 mg shift positively, which is possibly due to the electronegativity of C/N is relatively high, causing the lone pair of electrons on Ti atoms to shift to its own direction, and reducing the electron density on Ti atoms. The corresponding Ti atoms will strengthen the binding ability of extra-nuclear electrons, and the binding energy will be improved. The XPS C1s spectra of TNCD-15 mg and N-CDs were compared in Fig. 2c. The two curves show the same characteristic peaks located at ca. 284.7, 285.6, 286.5 and 288.7 eV, which belonged to C-C, C-N, C-O, and C═O, respectively. It is worth noting that the peaks of C-O and C═O are negatively shifted after the incorporation of N-CDs into the TiO_2, which may due to the combination of C in N-CDs and O in TiO_2, the difference in electronegativity causes a higher binding energy in C 1s spectra and a

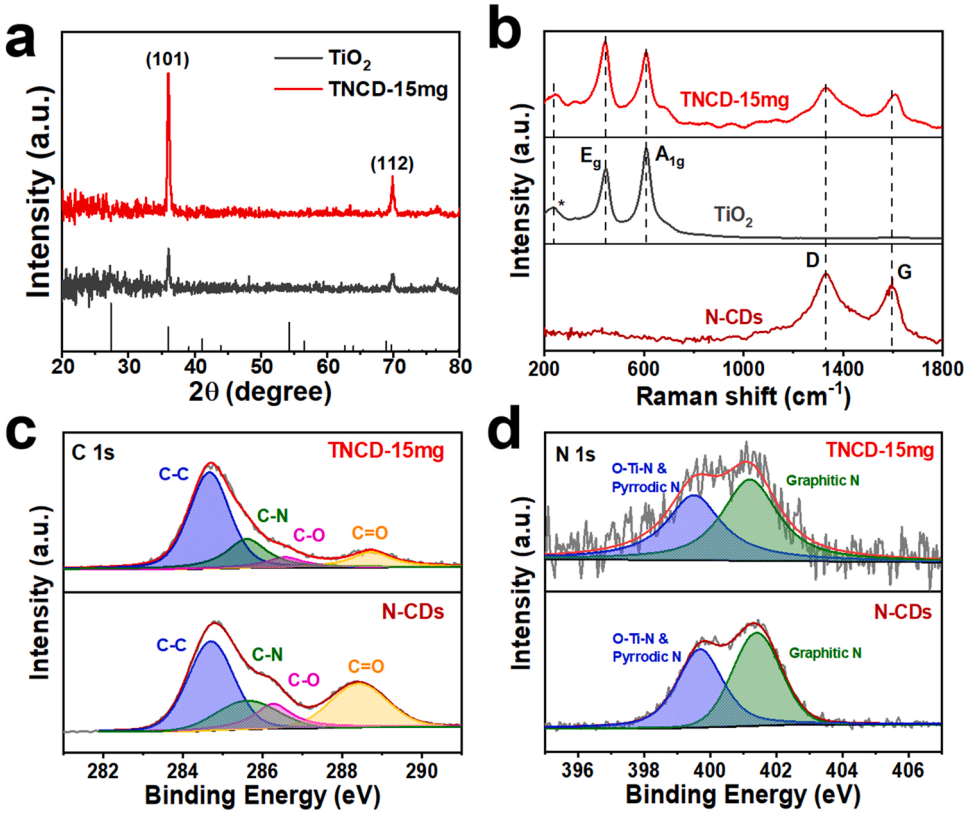

Fig. 2. (a) XRD patterns of TiO_2 and TNCD-15 mg. (b) Raman spectra of N-CDs, TiO_2 and TNCD-15 mg. The high resolution XPS spectra of C 1s (c) and N 1s (d).

lower binding energy in O 1s spectra (Fig. S5) [45].

In Fig. 2d, the chemical bonds of the N element of TNCD-15 mg and N-CDs are compared. On the curve of N-CDs, the peaks at ca. 399.7 and 401.4 eV are regarded as O-Ti-N/Pyrrodic N and Graphitic N [46,47], which are the same as the peaks of TNCD-15 mg. The above XPS spectrum results show that the N-CDs have been stably anchored in TiO_2.

Ultraviolet-visible absorption spectroscopy (UV–vis) was carried out to examine the optical performance and band structure of TNCD-15 mg and TiO_2. As shown in Fig. S6a, the absorption performance of TNCD-15 mg and TiO_2 in ultraviolet region is much better than visible light region, and the absorption edge of TiO_2 is located at ~ 410 nm, but it is worth mentioning that the anchored N-CDs caused a slight red shift in the UV–vis curve, thereby enhancing the absorption performance of TiO_2 in visible region [48]. Besides, the Tauc plot can be calculated by the Eq. (1):

$$(\alpha h\nu)^{1/n} = A\left(h\nu - E_g\right) \quad (1)$$

Where α means the absorbance index, h means the Planck constant, ν means the frequency, A means a constant and E_g means the band gap [49]. The calculated curves are shown in Fig. S6b, the E_g of TiO_2 and TNCD-15 mg are 2.83 and 2.80 eV respectively, indicating the N-CDs anchored can hardly change the band gap of TiO_2.

3.2. Photoelectrochemical properties of photoanodes

The schematic of the PEC cell is shown in Fig. 3a, in which the high-energy photons of the incoming solar irradiation are absorbed by a large-bandgap photoanode to generate photo-generated electron-holes pairs. Holes oxidize H_2O molecules at the photoanode to produce oxygen, while electrons were transfer to the cathode and underwent a reduction reaction with H^+ to produce H_2. The linear sweep voltammetric (LSV) curves of TiO_2 and TNCD-15 mg are shown in Fig. 3b, which indicates that the addition of N-CDs has an obvious effect on increasing the PEC performance. The maximum photocurrent density of TNCD-15 mg is increased by 2.2 times higher than that of the primitive TiO_2, and the onset potential (E_{on}) of TNCD-15 mg is decreased from that of TiO_2 by 0.022 V. Considering that a low onset potential of the photocurrent can reduce the external bias needed to reach the maximum photocurrent and improve the PEC efficiency on the whole, it makes sense to keep the onset potential as low as possible. In order to make a thorough inquiry of the relationship between the quality of N-CDs added and the properties of PEC, the samples that contained different quality of N-CDs have been synthesized and tested, and the results (Fig. S7 and Fig. S8) are compared in Fig. 3c. As the addition of N-CDs increases from 0 mg to 20 mg, the photocurrent density of the sample increases and reaches the maximum at 15 mg. Meanwhile, the onset potential shows a downward trend and is inversely proportional to the quality of N-CDs (Table S3), which may due to the change of conductivity caused by anchored N-CDs and will be explained later in combination with EIS tests. In summary, after comprehensive consideration, 15 mg N-CDs have the most obvious effect on the performance of TiO_2. As an effective method to measure the recombination rate of photo-generated electrons and holes, J-t curves (Fig. 3d) show the photoresponse of the TNCD-15 mg and TiO_2. As shown in Fig. 3**d**, the photocurrent density rapidly increases when there is the illumination of light and sharply returns to nearly zero when the xenon lamp is off, so it can be drawn a clear conclusion that the photoanode synthesized has good reproducibility when the light is turned on or off. Besides, the durability test was also carried out to prove the stability of TNCD-15 mg photoanode. As shown in Fig. S9, after continuous illumination for 15 h, TNCD-15 mg can maintain ~ 74% of its initial photocurrent. The photocurrent density decreases significantly from the initial time, but as the illumination time increases, the attenuation becomes less obvious.

Faradaic efficiency refers to the percentage of actual products and theoretical products, which can express the photoelectrochemical activity of the photoanode more intuitively. Therefore, a hydrogen gas chromatograph was used to measure the amount of H_2 released by Pt

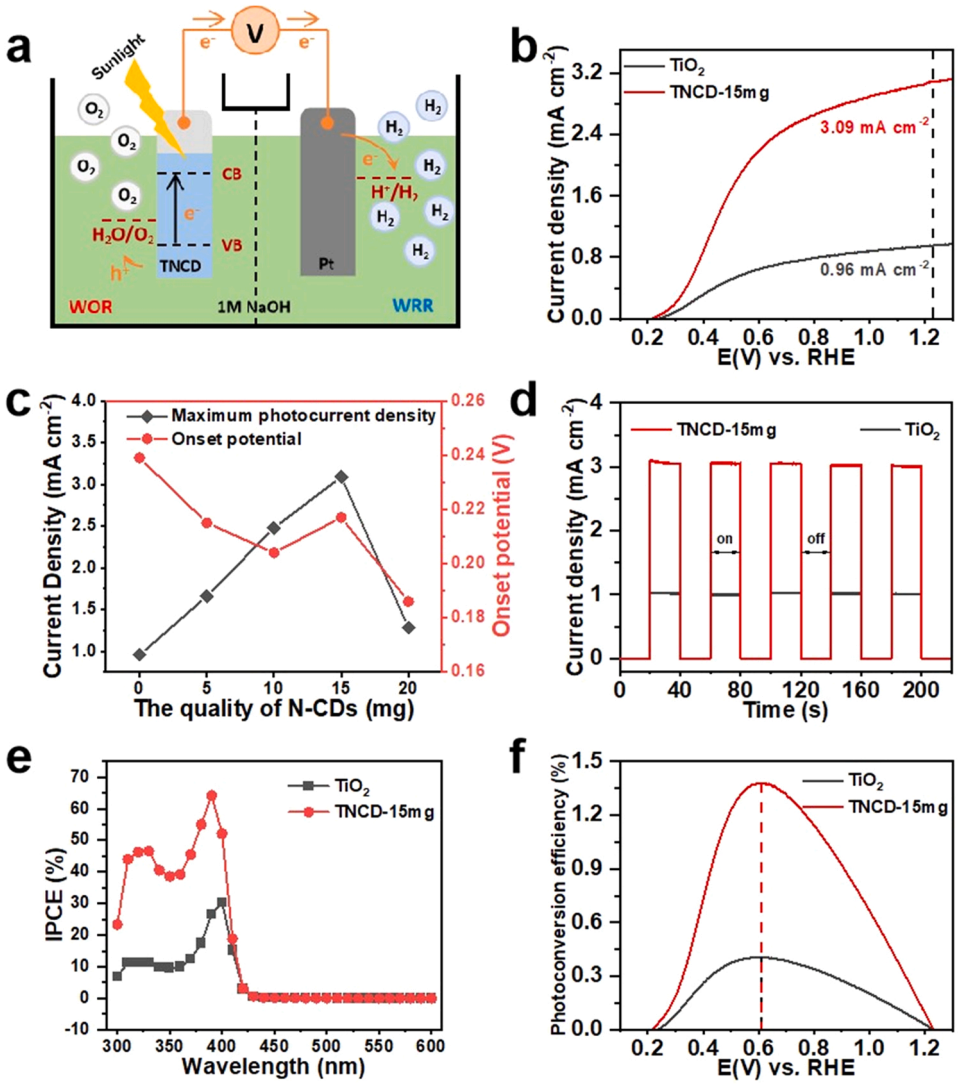

Fig. 3. (a) The schematic of PEC cell, (b) the LSV curves in 1.0 M NaOH, (c) the relationship between N-CDs quality and PEC performance, (d) photoresponse measured under chopped light illumination (AM 1.5 G) at 1.23 V vs. RHE, (e) IPCE spectra and (f) the calculated ABPE of TiO_2 and TNCD-15 mg.

cathode under light (Fig. S10). As shown, the H_2 produced by the Pt cathode is in good agreement with the theoretically calculated H_2 production. The faradaic efficiency was estimated to be ~94%, indicating that the TNCD-15 mg photoanode has excellent PEC hydrogen production performance for the Pt cathode. IPCE is considered to be one of the quantum efficiency metrics, which is beneficial to determine which photon energy contributes to the solar photocurrent [50]. λ is the wavelength of the monochromatic incident light, $J_{ph,\lambda}$ is the photocurrent density measured at each wavelength and P_λ is the respective incident power density. All the metrics above are measured at 1.23 V vs. RHE. Eventually, the IPCE can be calculated as Eq. (2):

$$IPCE_\lambda = J_{ph,\lambda} \times \frac{\frac{hc}{e}}{P_\lambda \times \lambda} \tag{2}$$

Where hc/e is equal to 1240 V nm [51]. As shown in Fig. 3e, TiO_2 and TNCD-15 mg both have high efficiency at less than ~ 430 nm, indicating that the addition of N-CDs does not change the fact that the photon-to-electron conversion of TiO_2 is concentrated in the ultraviolet region. Both TiO_2 and TNCD-15 mg exist the maximum IPCE value at ~ 390 nm, which reach ~ 30% and ~ 65%, respectively. Besides, the overall applied bias photon to current efficiency (ABPE) can be calculated as Eq. (3):

$$\eta = \frac{I(1.23 - V)}{J_{light}} \tag{3}$$

where V is the bias voltage vs. RHE, I is the photocurrent density at the measured potential, and J_{light} is the irradiance intensity [52]. As shown in Fig. 3f, both TiO_2 and TNCD-15 mg reach the saturation potential at 0.60 V vs. RHE, but the highest photoconversion efficiency of TNCD-15 mg is 1.38%, which is much higher than that of TiO_2 (0.4%), illustrating that the anchored N-CDs can significantly promote the maximum photocurrent at the same saturation potential, thereby greatly improving the light conversion efficiency. The clear increase in the efficiency of IPCE and ABPE can be inferred as the result of the effect that N-CDs act on electrons, that is, N-CDs reduce the recombination rate of photo-generated charges and holes, thereby the number of electrons produced in the external circuit per unit time, but the number of incident monochromatic photons per unit time does not change, so the two efficiencies mentioned above increase [53,54].

3.3. Mechanism of the photocatalytic process

Based on the conclusions drawn from the above performance analysis, we hypothesized a possible mechanism: the N-CDs anchored in

TNCD have the ability to bind electrons, like electron traps, which slow down the recombination speed of photo-generated electrons and holes. In order to prove this mechanism, the in-situ TPV test was carried out and the results are shown in Fig. 4. The relationship between PEC efficiencies and TPV parameters can be summarized in Fig. 4a. The in-situ TPV test of N-CDs is firstly conducted to research the effect of N-CDs themselves on the interface charges. As shown in Fig. 4b, the curve experiences a process of rising and then falling, which means the electron-hole pairs in the N-CDs are separated by light excitation and recombined. However, the curve continues to decline and begins to fall below the baseline at the moment of ~ 1.5 ms then rises to the baseline at the moment of ~ 3 ms. As previously reported [55], this phenomenon may be due to the formation of the electron-trap effect by anchoring N-CDs, so the electrons "captured" by the N-CDs cannot compound with the holes in the valence band in a short time. As a result, the electrons in the system are absorbed by the N-CDs, resulting in a negative signal on the TPV curve. Over time, the "captured" electrons gradually pass through the barrier and recombine with the holes, eventually reaching equilibrium. Significantly, the phenomenon of electron trap is also been observed in the curve of TNCD-15 mg (Fig. 4c), illustrating that the ability of N-CDs is given to the photoanode. Meanwhile, the TPV test of the control samples was also carried out to supplementary prove the electron trap mechanism. As shown in Fig. S11, with the increased quality of N-CDs, the area of TPV curve below the baseline gradually increases, which makes clear that the effect of electron trap is more and more obvious with the increase of the amount of N-CDs and this phenomenon may cause by superposition effect of different amount of N-CDs [56]. Fig. 4d shows the t_{max} and the integral area (S), t_{max} means the time photoanodes take for the curves to rise from the baseline to the apex and the S can be used to represent the maximum amount of charge excited. The t_{max} of TNCD-15 mg and TiO_2 are 0.099 ms and 0.201 ms respectively, showing TNCD-15 mg needs less time to extract the electrons. The S of TNCD-15 mg and TiO_2 are 0.08664 and 0.03333 respectively, illustrating N-CDs anchored can promote the maximum amount of photo-generated charge. Meanwhile, the change transfer rate can be calculated by dividing the integral area by t_{max}, and the results of TiO_2 and TNCD-15 mg are 0.1658 ms and 0.8752 ms. The increase in charge transfer rate may be attributed to the interaction between the functional groups on the N-CDs and the titanium dioxide molecule. Besides, as depicted in Fig. 4e, the time attenuation constants (τ) are fitted and the results of TiO_2 and TNCD-15 mg are 0.3842 ms and 0.2173 ms, which can be thought of TNCD-15 mg needs shorter time to make electrons and holes recombine. It should be noted that the charge transfer rate and the time attenuation constant are related to the surface conductivity of the photoanode, so the N-CDs anchored may reduce resistance of TiO_2. Finally, the time attenuation constants (τ) and charge

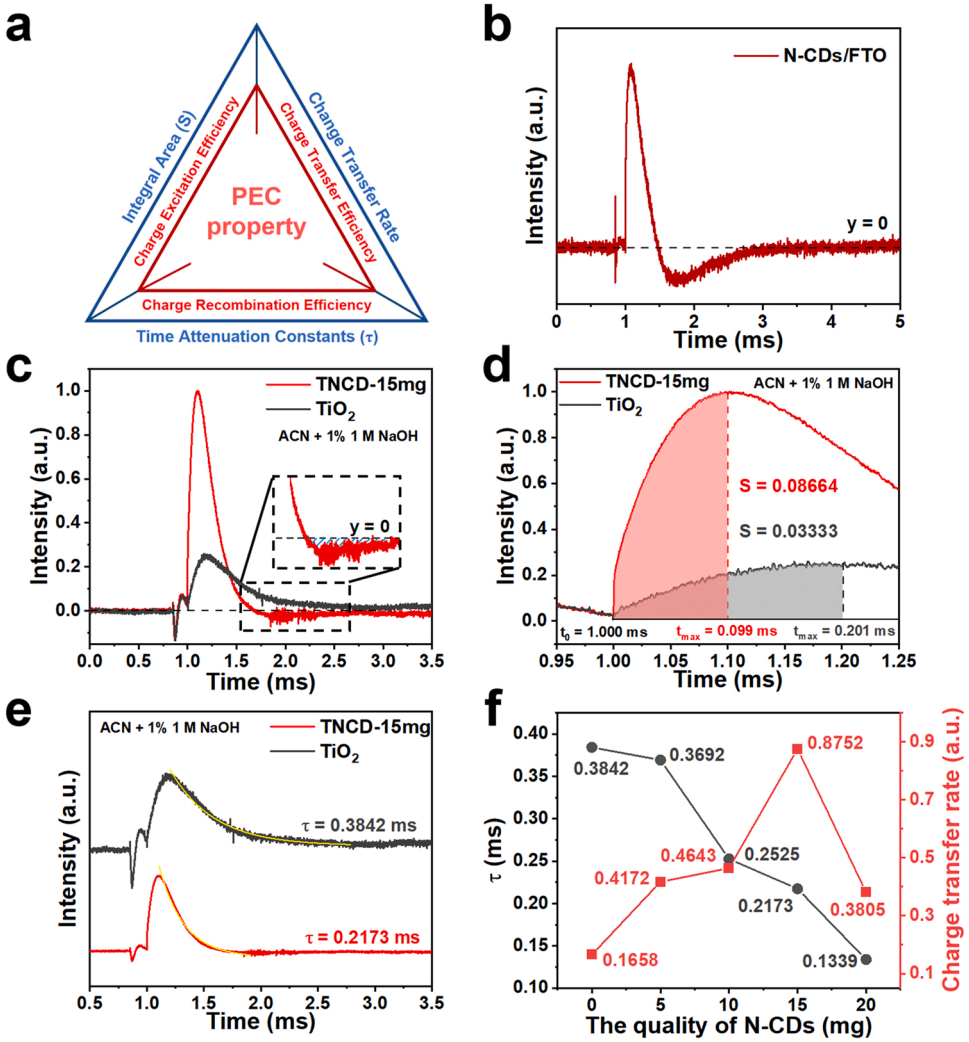

Fig. 4. (a) Relationship between PEC efficiencies and TPV parameters. The in-situ TPV curves of (b) N-CDs, (c) TiO_2 and TNCD-15 mg. (d) The maximum charge extraction time (t_{max}), the charge extraction process (S) and (e) charge recombination process (τ) of TiO_2 and TNCD-15 mg. (f) Relationship between N-CDs quality and TPV parameters.

transfer rate of the control samples are compared in Fig. 4f. The positive correlation between the quality of anchored N-CDs and τ can be inferred that more N-CDs leads to greater conductivity of the photoanode, so the time required for electron transfer to holes is shortened. The charge transfer rate of TNCD-15 mg is higher than that of control samples, indicating the charge transfer efficiency is affected by many factors, but its tendency can correspond well to the PEC performance.

Finally, the TPV parameters of other samples are compared in Fig. 4f, it can be seen that N-CDs anchored TiO_2 makes conductivity of TiO_2 increase generally and 15 mg N-CDs is the most obvious to increase the charge transfer rate.

To further study the interface electron transfer kinetics, the TPV signal of TNCD-15 mg and TiO_2 is analyzed by Fourier Transform (FFT) and Continuous wavelet transform (CWT). FFT is a tool that decomposes a waveform (function or signal) into alternate representations, characterized by sine and cosine. The result of FFT on the TNCD-15 mg TPV relaxation curve (red curve in Fig. 4c) is shown in Fig. 5a. This curve shows the maximum amplitude when the frequency is approximate to zero. A very smooth curve without any obvious peak indicates that there is no obvious static and periodic frequency components present in this TPV relaxation signal. Both the curve feature of the TPV signal and FFT results suggest that the TPV curve has obvious non-static characteristics. CWT is a Frequency-Time transform used to analyze non-static signals. In our system, the TPV relaxation curve is a typical non-static signal. Here, the continuous wavelet analysis with bior 3.9 as base function to analyze the time-frequency characteristics of these TPV curves. The CWT pattern of TNCD-15 mg TPV relaxation curve (red curve in Fig. 4c) is shown in Fig. 5b. Besides, more FFT and CWT analyses on the TPV signals of TiO_2 and TNCD-15 mg catalysts are shown in Fig. S12-S14.

As shown in Fig. S15, the Intensity-Frequency spectra reveal the distribution of electron transfer velocity in the sample at a certain moment. At t = 0.1 ms, the maximum electron transfer speed of TNCD-15 mg is 212 Hz while that of TiO_2 is 103 Hz. At t = 0.3 Hz, the maximum electron transfer speed of TNCD-15 mg is 97 Hz while that of TiO_2 is 70 Hz. And at t = 0.85 ms, the maximum electron transfer speed of TNCD-15 mg is 43 Hz while that of TiO_2 is 34 Hz. This result can be attributed to the stable combination of N-CDs and photoanode through carboxyl groups, which reduces the internal resistance of photoanode and makes the speed of charge separation and transfer faster. Therefore, the presence of N-CDs enables a faster electron transfer process inside the photoanode. Meanwhile, in Fig. 5c, the peak positions of intensity-time curves of TiO_2 and TNCD-15 mg at a frequency of 50 Hz are compared, and the negative shift of peak positions on the time scale after anchoring N-CDs can be observed. At each frequency, we calculate the average of the sets of time differences, and the results are shown in Fig. 5d (detailed calculation shown in supporting information). At 10–30 Hz, the peak delay time $\Delta t > 0$, and at 40–200 Hz, $\Delta t < 0$, indicating N-CDs make the slow process slower and the fast process

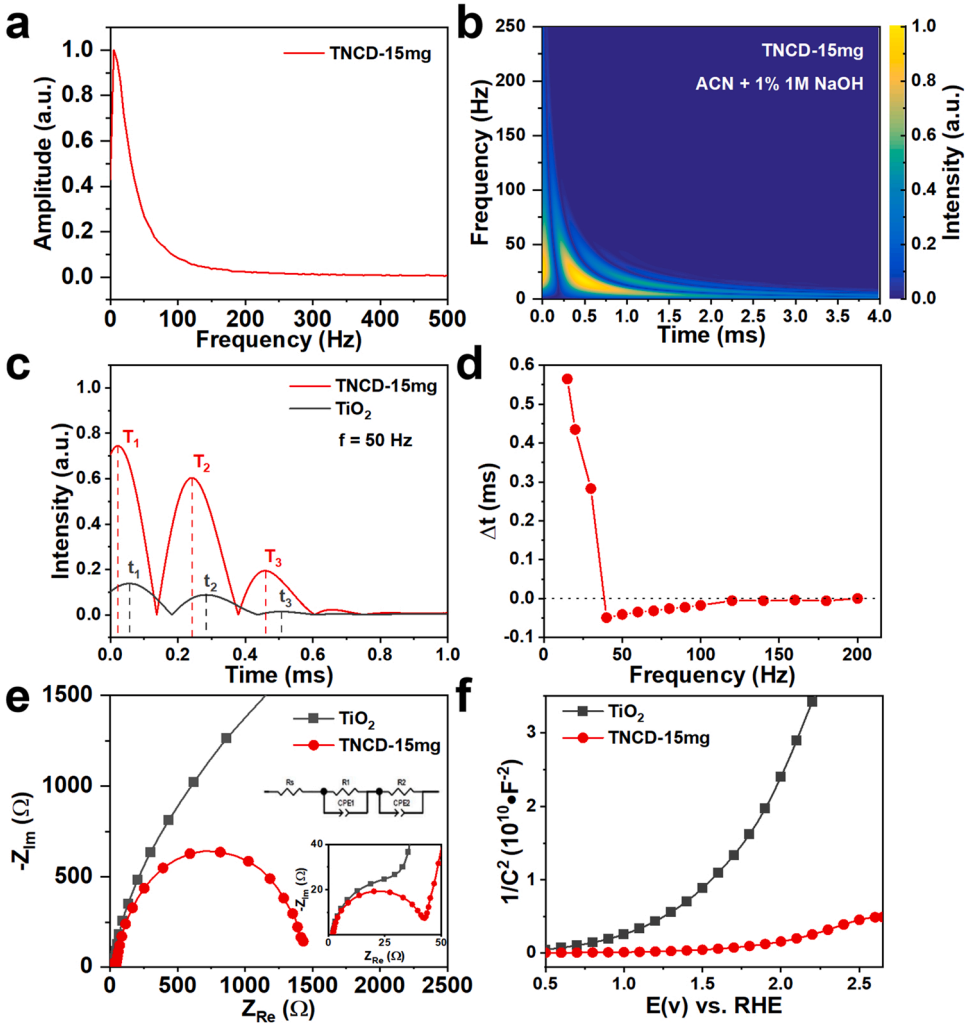

Fig. 5. (a) FFT spectrum, (b) 2D CWT spectrum, (c) Intensity-Frequency spectra (t = 0.1 ms, 0.3 ms and 0.85 ms) of TiO_2 and TNCD-15 mg, (d) peak delay time (Δt) at different frequencies of TiO_2 and TNCD-15 mg, (e) the electrical impedance spectroscopy (EIS) of TiO_2 and TNCD-15 mg, (f) Mott-Schottky plots of TiO_2 and TNCD-15 mg.

faster. Based on all the above data, it should be concluded that N-CDs may accelerate the interface electron extraction (fast process) by about 0.05 ms, while the maximum electron storage (slow process) time by CDs is up to 0.56 ms.

Then, the electrical impedance spectroscopy (EIS), Mott-Schottky plots and time-resolved fluorescence spectrum (TRPL) were conducted to confirm the conclusion of in-situ TPV and CWT. Fig. 5e shows the electrochemical impedance of TiO_2 and TNCD-15 mg, and both the curves can be fitted by the equivalent circuit inset. Corresponding to the equivalent circuit, the first arc (high frequency region) of the Nyquist plot is commonly used to describe the resistance within the photoanode (R_1) [57], while the second arc (low frequency region) corresponds to the charge transport through the interface of photoanode-electrolyte (R_2) [58]. Therefore, either interface impedance or internal impedance of photoanode, TNCD-15 mg is better than primitive TiO_2 (The electrochemical impedance of control samples and the specific parameters fitted from EIS are shown in Fig. S16 and Table S4). Meanwhile, compared tendencies of the resistance within the photoanode and E_{on} (Table S3), it can be inferred that E_{on} is positively correlated with the internal resistance of photoanodes and the anchored N-CDs increase the conductivity of the photoanodes themselves, thereby reducing the E_{on} [59].

The Mott-Schottky plots of TiO_2, TNCD-15 mg and control samples are shown in Fig. 5f and Fig. S17. Both the curves show positive slopes, indicating the samples are all n-type semiconductor characteristics. Meanwhile, TNCD-15 mg exhibits smaller slopes than that of TiO_2, suggesting doping increases the carrier density inside the sample, which can be calculated through the Mott-Schottky plots by the Eq. (4).

$$N_d = \frac{2}{e_0 \varepsilon \varepsilon_0} \times \frac{dV}{d\left(\frac{1}{C^2}\right)} \tag{4}$$

where e_0 equal to 1.602×10^{-19} C is the electron charge, ε equal to 170 represents the dielectric constant, ε_0 equal to 8.85×10^{-12} N^{-1} C^2 m^{-2} represents the vacuum permittivity. The other parameters like N_d are the carrier density, and V is the potential at the electrode [60]. The calculated results of TiO_2 and TNCD-15 mg are 1.49×10^{16} cm^{-3} and 1.36×10^{17} cm^{-3} respectively (Table S5), illustrating the anchored N-CDs increase the carrier density of TiO_2 photoanode and this result is tally with the comparison of the integral areas of the two photoanodes in in-situ TPV tests.

To explore carrier recombination dynamics, time-resolved PL spectra (TRPL) were utilized (Fig. S18). The double exponential function of time (t) can fit the TRPL curve well by the Eq. (5).

$$F(t) = A_1 e^{-\frac{1}{\tau_1}} + A_2 e^{-\frac{1}{\tau_2}} + \gamma_0 \tag{5}$$

Where τ_1 refers to the time constant of the fast decay process and τ_2 refers to that of slow decay process [61]. The surface recombination influences the fast decay, while the electron-hole recombination in the bulk of the TiO_2 films influences the slow decay. The average lifetime can be calculated by the Eq. (6) [61]:

$$\tau_{avg} = \frac{A_1\tau_1^2 + A_2\tau_2^2}{A_1\tau_1 + A_2\tau_2} \tag{6}$$

The fitting results reveal that TNCD-15 mg has a shorter average lifetime (3.5307 ns) than that of TiO_2 (3.8498 ns), indicating the N-CDs anchored can slightly increase the charge transfer of recombination in the TiO_2, which also conform to the results of TPV.

Scheme 1 proposes a possible reaction mechanism. Under the illumination of solar light, TNCD-15 mg can easily generate photo-generated electron-hole pairs. The photo-generated electrons quickly conduct to N-CDs then transfer to the counter electrode, meanwhile the photo-generated holes remain on the TiO_2 nanorods and react with H_2O to produce O_2. During this charge transfer process, due to the existence of N-CDs, the fast electron transfer process becomes faster, promoting the charge transfer efficiency. Simultaneously, the formation of electron-trap effect by anchoring N-CDs in TiO_2 photoanode causes the slow electron transfer process to be even slower, promoting the surface redox reaction rate and further improving the surface charge injection efficiency.

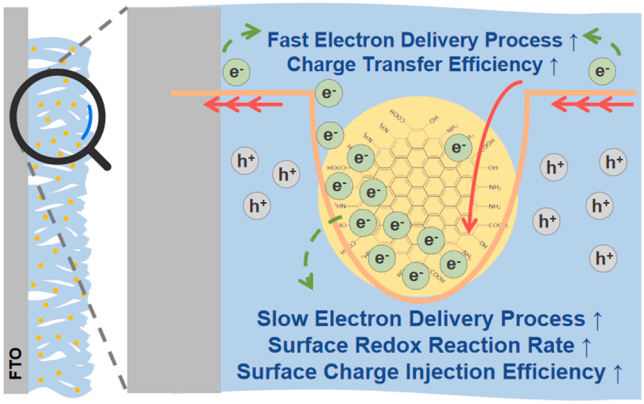

Scheme 1. Schematic mechanism of the effect of carbon dots in TNCD-15 mg photoanode.

4. Conclusion

The TiO_2 photoanode was modified by N-CDs through one-step hydrothermal method. This kind of photoanodes, such as TNCD-15 mg, show improved photoelectrochemical catalytic performance. The in-situ TPV study suggests that electron-trap effect is formed in TiO_2 photoanode due to the existence of N-CDs, which improves the efficiency of photo-generated charge separation. Meanwhile, N-CDs increasing the conductivity of TiO_2 photoanode and improving the efficiency of photo-generated charge transfer are proven. Under AM 1.5 G light intensity and 1.23 V vs. RHE, the photocurrent density of TNCD-15 mg is 3.09 mA cm^{-2} in 1.0 M NaOH, which is ~ 3.22 times of that of the primitive TiO_2 and is at a high level in recent reports (Fig. S19). This work provides a new idea for PEC material design to achieve higher PEC performances.

CRediT authorship contribution statement

Yidong Han: Data curation, Visualization. **Jie Wu:** Formal analysis. **Yi Li:** Investigation, Software. **Xiaoqing Gu:** Investigation. **Tiwei He:** Software. **Yu Zhao:** Writing – original draft, **Hui Huang:** Project administration, Writing – original draft, Writing – review & editing, Supervision, **Yang Liu:** Resources, Writing – review & editing, Supervision, **Zhenhui Kang:** Conceptualization, Funding acquisition, Writing – review & editing, Supervision.

Declaration of Competing Interest

The authors report no declarations of interest.

Acknowledgements

This work is supported by National Key Research and Development Project of China (2020YFA0406101, 2020YFA0406104), National MCF Energy R&D Program (2018YFE0306105), Key-Area Research and Development Program of GuangDong Province (2019B010933001), Innovative Research Group Project of the National Natural Science Foundation of China (51821002), National Natural Science Foundation of China (51725204, 21771132, 51972216, 52041202), Natural Science Foundation of Jiangsu Province (BK20190041), Collaborative Innovation Center of Suzhou Nano Science & Technology, the 111 Project and

Suzhou Key Laboratory of Functional Nano & Soft Materials.

Appendix A. Supporting information

Supplementary data associated with this article can be found in the online version at doi:10.1016/j.apcatb.2021.120983.

References

[1] W. Yang, R.R. Prabhakar, J. Tan, S.D. Tilley, J. Moon, Strategies for enhancing the photocurrent, photovoltage, and stability of photoelectrodes for photoelectrochemical water splitting, Chem. Soc. Rev. 48 (2019) 4979–5015, https://doi.org/10.1039/c8cs00997j.

[2] S. Singh, H. Chen, S. Shahrokhi, L.P. Wang, C.-H. Lin, L. Hu, X. Guan, A. Tricoli, Z. J. Xu, T. Wu, Hybrid organic–inorganic materials and composites for photoelectrochemical water splitting, ACS Energy Lett. 5 (2020) 1487–1497, https://doi.org/10.1021/acsenergylett.0c00327.

[3] E. Romero, V.I. Novoderezhkin, R. van Grondelle, Quantum design of photosynthesis for bio-inspired solar-energy conversion, Nature 543 (2017) 355–365, https://doi.org/10.1038/nature22012.

[4] M. Gratzel, Photoelectrochemical cells, Nature 414 (2001) 338–344, https://doi.org/10.1038/35104607.

[5] R. Passalacqua, S. Perathoner, G. Centi, Semiconductor, molecular and hybrid systems for photoelectrochemical solar fuel production, J. Energy Chem. 26 (2017) 219–240, https://doi.org/10.1016/j.jechem.2017.03.004.

[6] Y. Qiu, Z. Pan, H. Chen, D. Ye, L. Guo, Z. Fan, S. Yang, Current progress in developing metal oxide nanoarrays-based photoanodes for photoelectrochemical water splitting, Sci. Bull. 64 (2019) 1348–1380, https://doi.org/10.1016/j.scib.2019.07.017.

[7] Y. Liu, B.R. Wygant, K. Kawashima, O. Mabayoje, T.E. Hong, S.-G. Lee, J. Lin, J.-H. Kim, K. Yubuta, W. Li, J. Li, C.B. Mullins, Facet effect on the photoelectrochemical performance of a WO_3/$BiVO_4$ heterojunction photoanode, Appl. Catal. B 245 (2019) 227–239, https://doi.org/10.1016/j.apcatb.2018.12.058.

[8] C. Fàbrega, S. Murcia-López, D. Monllor-Satoca, J.D. Prades, M.D. Hernández-Alonso, G. Penelas, J.R. Morante, T. Andreu, Efficient WO_3 photoanodes fabricated by pulsed laser deposition for photoelectrochemical water splitting with high faradaic efficiency, Appl. Catal. B 189 (2016) 133–140, https://doi.org/10.1016/j.apcatb.2016.02.047.

[9] R. Chong, Y. Du, Z. Chang, Y. Jia, Y. Qiao, S. Liu, Y. Liu, Y. Zhou, D. Li, 2D Co-incorporated hydroxyapatite nanoarchitecture as a potential efficient oxygen evolution cocatalyst for boosting photoelectrochemical water splitting on Fe_2O_3 photoanode, Appl. Catal. B 250 (2019) 224–233, https://doi.org/10.1016/j.apcatb.2019.03.038.

[10] H.-J. Ahn, K.-Y. Yoon, M.-J. Kwak, J. Park, J.-H. Jang, Boron doping of metal-doped hematite for reduced surface recombination in water splitting, ACS Catal. 8 (2018) 11932–11939, https://doi.org/10.1021/acscatal.8b03184.

[11] S.A. Monny, Z. Wang, M. Konarova, L. Wang, Bismuth based photoelectrodes for solar water splitting, J. Energy Chem. 61 (2021) 517–530, https://doi.org/10.1016/j.jechem.2021.01.047.

[12] H.S. Han, S. Shin, D.H. Kim, I.J. Park, J.S. Kim, P.-S. Huang, J.-K. Lee, I.S. Cho, X. Zheng, Boosting the solar water oxidation performance of a $BiVO_4$ photoanode by crystallographic orientation control, Energy Environ. Sci. 11 (2018) 1299–1306, https://doi.org/10.1039/c8ee00125a.

[13] L. Pan, J.H. Kim, M.T. Mayer, M.-K. Son, A. Ummadisingu, J.S. Lee, A. Hagfeldt, J. Luo, M. Grätzel, Boosting the performance of Cu_2O photocathodes for unassisted solar water splitting devices, Nat. Catal. 1 (2018) 412–420, https://doi.org/10.1038/s41929-018-0077-6.

[14] L. Yang, Z. Li, H. Jiang, W. Jiang, R. Su, S. Luo, Y. Luo, Photoelectrocatalytic oxidation of bisphenol A over mesh of TiO_2/graphene/Cu_2O, Appl. Catal. B 183 (2016) 75–85, https://doi.org/10.1016/j.apcatb.2015.10.023.

[15] A. Bayat, E. Saievar-Iranizad, Graphene quantum dots decorated rutile TiO_2 nanoflowers for water splitting application, J. Energy Chem. 27 (2018) 306–310, https://doi.org/10.1016/j.jechem.2017.09.036.

[16] T. Zhou, S. Chen, L. Li, J. Wang, Y. Zhang, J. Li, J. Bai, L. Xia, Q. Xu, M. Rahim, B. Zhou, Carbon quantum dots modified anatase/rutile TiO_2 photoanode with dramatically enhanced photoelectrochemical performance, Appl. Catal. B 269 (2020), https://doi.org/10.1016/j.apcatb.2020.118776.

[17] Q. Guo, C. Zhou, Z. Ma, X. Yang, Fundamentals of TiO_2 photocatalysis: concepts, mechanisms, and challenges, Adv. Mater. 31 (2019), e1901997, https://doi.org/10.1002/adma.201901997.

[18] G.L. Chiarello, M.V. Dozzi, E. Selli, TiO_2-based materials for photocatalytic hydrogen production, J. Energy Chem. 26 (2017) 250–258, https://doi.org/10.1016/j.jechem.2017.02.005.

[19] J.W. Yoon, D.H. Kim, J.-H. Kim, H.W. Jang, J.-H. Lee, NH_2-MIL-125(Ti)/TiO_2 nanorod heterojunction photoanodes for efficient photoelectrochemical water splitting, Appl. Catal. B 244 (2019) 511–518, https://doi.org/10.1016/j.apcatb.2018.11.057.

[20] X. Song, W. Li, D. He, H. Wu, Z. Ke, C. Jiang, G. Wang, X. Xiao, The "Midas Touch" transformation of TiO_2 nanowire arrays during visible light photoelectrochemical performance by carbon/nitrogen coimplantation, Adv. Energy Mater. 8 (2018), 1800165, https://doi.org/10.1002/aenm.201800165.

[21] E.M. Neville, J.M.D. MacElroy, K.R. Thampi, J.A. Sullivan, Visible light active C-doped titanate nanotubes prepared via alkaline hydrothermal treatment of C-doped nanoparticulate TiO_2: photo-electrochemical and photocatalytic properties, J. Photochem. Photobiol. A 267 (2013) 17–24, https://doi.org/10.1016/j.jphotochem.2013.06.008.

[22] C. Wang, Z. Chen, H. Jin, C. Cao, J. Li, Z. Mi, Enhancing visible-light photoelectrochemical water splitting through transition-metal doped TiO_2 nanorod arrays, J. Mater. Chem. A 2 (2014) 17820–17827, https://doi.org/10.1039/c4ta04254a.

[23] J. Li, D. Wang, R. Guan, Y. Zhang, Z. Zhao, H. Zhai, Z. Sun, Vacancy-enabled mesoporous TiO_2 modulated by nickel doping with enhanced photocatalytic nitrogen fixation performance, ACS Sustain. Chem. Eng. 8 (2020) 18258–18265, https://doi.org/10.1021/acssuschemeng.0c06775.

[24] A. Sengele, D. Robert, N. Keller, C. Colbeau-Justin, V. Keller, Sn-doped and porogen-modified TiO_2 photocatalyst for solar light elimination of sulfure diethyle as a model for chemical warfare agent, Appl. Catal. B 245 (2019) 279–289, https://doi.org/10.1016/j.apcatb.2018.12.071.

[25] C.J. Lin, Y.H. Liou, Y. Zhang, C.L. Chen, C.-L. Dong, S.-Y. Chen, G.D. Stucky, Mesoporous Fe-doped TiO_2 sub-microspheres with enhanced photocatalytic activity under visible light illumination, Appl. Catal. B 127 (2012) 175–181, https://doi.org/10.1016/j.apcatb.2012.08.011.

[26] W. Fang, M. Xing, J. Zhang, A new approach to prepare Ti^{3+} self-doped TiO_2 via $NaBH_4$ reduction and hydrochloric acid treatment, Appl. Catal. B 160–161 (2014) 240–246, https://doi.org/10.1016/j.apcatb.2014.05.031.

[27] N.C.T. Martins, J. Ângelo, A.V. Girão, T. Trindade, L. Andrade, A. Mendes, N-doped carbon quantum dots/TiO_2 composite with improved photocatalytic activity, Appl. Catal. B 193 (2016) 67–74, https://doi.org/10.1016/j.apcatb.2016.04.016.

[28] Z. Xie, X. Liu, W. Wang, X. Wang, C. Liu, Q. Xie, Z. Li, Z. Zhang, Enhanced photoelectrochemical and photocatalytic performance of TiO_2 nanorod arrays/CdS quantum dots by coating TiO_2 through atomic layer deposition, Nano Energy 11 (2015) 400–408, https://doi.org/10.1016/j.nanoen.2014.11.024.

[29] W.T. Sun, Y. Yu, H.Y. Pan, X.F. Gao, Q. Chen, L.M. Peng, CdS quantum dots sensitized TiO_2 nanotube-array photoelectrodes, J. Am. Chem. Soc. 130 (2008) 1124–1125, https://doi.org/10.1021/ja0777741.

[30] G.A.M. Hutton, B.C.M. Martindale, E. Reisner, Carbon dots as photosensitisers for solar-driven catalysis, Chem. Soc. Rev. 46 (2017) 6111–6123, https://doi.org/10.1039/c7cs00235a.

[31] H. Zhao, X. Yu, C.-F. Li, W. Yu, A. Wang, Z.-Y. Hu, S. Larter, Y. Li, M. Golam Kibria, J. Hu, Carbon quantum dots modified TiO_2 composites for hydrogen production and selective glucose photoreforming, J. Energy Chem. 64 (2022) 201–208, https://doi.org/10.1016/j.jechem.2021.04.033.

[32] J. Bian, C. Huang, L. Wang, T. Hung, W.A. Daoud, R. Zhang, Carbon dot loading and TiO_2 nanorod length dependence of photoelectrochemical properties in carbon dot/TiO_2 nanorod array nanocomposites, ACS Appl. Mater. Interfaces 6 (2014) 4883–4890, https://doi.org/10.1021/am4059183.

[33] H. Luo, S. Dimitrov, M. Daboczi, J.-S. Kim, Q. Guo, Y. Fang, M.-A. Stoeckel, P. Samorì, O. Fenwick, A.B. Jorge Sobrido, X. Wang, M.-M. Titirici, Nitrogen-doped carbon dots/TiO_2 nanoparticle composites for photoelectrochemical water oxidation, ACS Appl. Nano Mater. 3 (2020) 3371–3381, https://doi.org/10.1021/acsanm.9b02412.

[34] Z. Liang, H. Hou, Z. Fang, F. Gao, L. Wang, D. Chen, W. Yang, Hydrogenated TiO_2 nanorod arrays decorated with carbon quantum dots toward efficient photoelectrochemical water splitting, ACS Appl. Mater. Interfaces 11 (2019) 19167–19175, https://doi.org/10.1021/acsami.9b04059.

[35] Y. Liu, L. Zhou, Y. Li, R. Deng, H. Zhang, Highly fluorescent nitrogen-doped carbon dots with excellent thermal and photo stability applied as invisible ink for loading important information and anti-counterfeiting, Nanoscale 9 (2017) 491–496, https://doi.org/10.1039/c6nr07123f.

[36] F. Wang, P. Chen, Y. Feng, Z. Xie, Y. Liu, Y. Su, Q. Zhang, Y. Wang, K. Yao, W. Lv, G. Liu, Facile synthesis of N-doped carbon dots/g-C_3N_4 photocatalyst with enhanced visible-light photocatalytic activity for the degradation of indomethacin, Appl. Catal. B 207 (2017) 103–113, https://doi.org/10.1016/j.apcatb.2017.02.024.

[37] T. Toyoda, Q. Shen, Quantum-dot-sensitized solar cells: effect of nanostructured TiO2 morphologies on photovoltaic properties, J. Phys. Chem. Lett. 3 (2012) 1885–1893, https://doi.org/10.1021/jz3004602.

[38] S. Hu, W. Yang, N. Li, H. Wang, J. Yang, Q. Chang, Carbon-dot-based heterojunction for engineering band-edge position and photocatalytic performance, Small 14 (2018), e1803447, https://doi.org/10.1002/smll.201803447.

[39] Y. Li, Y. Zhao, H. Nie, K. Wei, J. Cao, H. Huang, M. Shao, Y. Liu, Z. Kang, Interface photo-charge kinetics regulation by carbon dots for efficient hydrogen peroxide production, J. Mater. Chem. A 9 (2021) 515–522, https://doi.org/10.1039/d0ta10231h.

[40] H.G. Yang, C.H. Sun, S.Z. Qiao, J. Zou, G. Liu, S.C. Smith, H.M. Cheng, G.Q. Lu, Anatase TiO_2 single crystals with a large percentage of reactive facets, Nature 453 (2008) 638–641, https://doi.org/10.1038/nature06964.

[41] A. McLaren, T. Valdes-Solis, G. Li, S.C. Tsang, Shape and size effects of ZnO nanocrystals on photocatalytic activity, J. Am. Chem. Soc. 131 (2009) 12540–12541, https://doi.org/10.1021/ja9052703.

[42] M. Feng, Y. Liu, N. Wei, S. Ma, Z. Li, H. Li, S. Chen, J. Liu, D. Wang, Alumina anchored CQDs/TiO2 nanorods by atomic layer deposition for efficient photoelectrochemical water splitting under solar light, J. Mater. Chem. A 6 (2018) 18293–18303, https://doi.org/10.1039/c8ta05092a.

[43] M.P. Suryawanshi, U.V. Ghorpade, S.W. Shin, M.G. Gang, X. Wang, H. Park, S. H. Kang, J.H. Kim, Enhanced solar water oxidation performance of TiO_2 via band

edge engineering: a tale of sulfur doping and earth-abundant czts nanoparticles sensitization, ACS Catal. 7 (2017) 8077–8089, https://doi.org/10.1021/acscatal.7b02102.
[44] S.S.M. Bhat, S.A. Pawar, D. Potphode, C.-K. Moon, J.M. Suh, C. Kim, S. Choi, D. S. Patil, J.-J. Kim, J.C. Shin, H.W. Jang, Substantially enhanced photoelectrochemical performance of TiO_2 nanorods/CdS nanocrystals heterojunction photoanode decorated with MoS_2 nanosheets, Appl. Catal., B 259 (2019), 118261, https://doi.org/10.1016/j.apcatb.2019.118102.
[45] J. Yang, H. Bai, X. Tan, J. Lian, IR and XPS investigation of visible-light photocatalysis—Nitrogen–carbon-doped TiO_2 film, Appl. Surf. Sci. 253 (2006) 1988–1994, https://doi.org/10.1016/j.apsusc.2006.03.078.
[46] H. Wang, M. Zhang, Y. Song, H. Li, H. Huang, M. Shao, Y. Liu, Z. Kang, Carbon dots promote the growth and photosynthesis of mung bean sprouts, Carbon 136 (2018) 94–102, https://doi.org/10.1016/j.carbon.2018.04.051.
[47] H. Han, F. Karlicky, S. Pitchaimuthu, S.H.R. Shin, A. Chen, Highly ordered N-doped carbon dots photosensitizer on metal-organic framework-decorated zno nanotubes for improved photoelectrochemical water splitting, Small 15 (2019), e1902771, https://doi.org/10.1002/smll.201902771.
[48] C. Hou, H. Liu, Y. Li, The preparation of three-dimensional flower-like TiO_2/$TiOF_2$ photocatalyst and its efficient degradation of tetracycline hydrochloride, RSC Adv. 11 (2021) 14957–14969, https://doi.org/10.1039/d1ra01772a.
[49] H.L. Tan, F.F. Abdi, Y.H. Ng, Heterogeneous photocatalysts: an overview of classic and modern approaches for optical, electronic, and charge dynamics evaluation, Chem. Soc. Rev. 48 (2019) 1255–1271, https://doi.org/10.1039/c8cs00882e.
[50] K. Sivula, R. van de Krol, Erratum: semiconducting materials for photoelectrochemical energy conversion, Nat. Rev. Mater. (2016) 15010, https://doi.org/10.1038/natrevmats.2016.10.
[51] P. Zhang, X.F. Lu, D. Luan, X.W.D. Lou, Fabrication of heterostructured Fe_2TiO_5 -TiO_2 nanocages with enhanced photoelectrochemical performance for solar energy conversion, Angew. Chem. Int. Ed. 59 (2020) 8128–8132, https://doi.org/10.1002/anie.202000697.
[52] T. Zhou, J. Wang, S. Chen, J. Bai, J. Li, Y. Zhang, L. Li, L. Xia, M. Rahim, Q. Xu, B. Zhou, Bird-nest structured ZnO/TiO_2 as a direct Z-scheme photoanode with enhanced light harvesting and carriers kinetics for highly efficient and stable photoelectrochemical water splitting, Appl. Catal. B 267 (2020), https://doi.org/10.1016/j.apcatb.2020.118599.
[53] Q. Chai, W. Li, Y. Wu, K. Pei, J. Liu, Z. Geng, H. Tian, W. Zhu, Effect of a long alkyl group on cyclopentadithiophene as a conjugated bridge for D-A-pi-A organic sensitizers: IPCE, electron diffusion length, and charge recombination, ACS Appl. Mater. Interfaces 6 (2014) 14621–14630, https://doi.org/10.1021/am503891q.
[54] H. Li, C. Xie, Y. Liao, Y. Liu, Z. Zou, J. Wu, Characterization of incidental photon-to-electron conversion efficiency (IPCE) of porous TiO_2/SnO_2 composite film, J. Alloy. Compd. 569 (2013) 88–94, https://doi.org/10.1016/j.jallcom.2013.03.126.
[55] Q. Wu, J. Cao, X. Wang, Y. Liu, Y. Zhao, H. Wang, Y. Liu, H. Huang, F. Liao, M. Shao, Z. Kang, A metal-free photocatalyst for highly efficient hydrogen peroxide photoproduction in real seawater, Nat. Commun. 12 (2021) 483, https://doi.org/10.1038/s41467-020-20823-8.
[56] Q. Chen, Y. Liu, X. Gu, D. Li, D. Zhang, D. Zhang, H. Huang, B. Mao, Z. Kang, W. Shi, Carbon dots mediated charge sinking effect for boosting hydrogen evolution in Cu-In-Zn-S QDs/MoS_2 photocatalysts, Appl. Catal. B 301 (2022), 120755, https://doi.org/10.1016/j.apcatb.2021.120755.
[57] C. Hou, H. Liu, F.B. Mohammad, Preparation of ordered mesoporous F–$H_2Ti_3O_7$ nanosheets using orthorhombic $HTiOF_3$ as a precursor and their highly efficient degradation of tetracycline hydrochloride under simulated sunlight, J. Solid State Chem. 300 (2021), https://doi.org/10.1016/j.jssc.2021.122288.
[58] C.S. Chua, D. Ansovini, C.J. Lee, Y.T. Teng, L.T. Ong, D. Chi, T.S. Hor, R. Raja, Y. F. Lim, The effect of crystallinity on photocatalytic performance of Co_3O_4 water-splitting cocatalysts, Phys. Chem. Chem. Phys. 18 (2016) 5172–5178, https://doi.org/10.1039/c5cp07589k.
[59] J. Hojberg, B.D. McCloskey, J. Hjelm, T. Vegge, K. Johansen, P. Norby, A.C. Luntz, An electrochemical impedance spectroscopy investigation of the overpotentials in Li-O_2 batteries, ACS Appl. Mater. Interfaces 7 (2015) 4039–4047, https://doi.org/10.1021/am5083254.
[60] S. Zhang, M. Li, J. Zhao, H. Wang, X. Zhu, J. Han, X. Liu, Plasmonic AuPd-based Mott-Schottky photocatalyst for synergistically enhanced hydrogen evolution from formic acid and aldehyde, Appl. Catal. B 252 (2019) 24–32, https://doi.org/10.1016/j.apcatb.2019.04.013.
[61] C. Zhou, C. Lai, D. Huang, G. Zeng, C. Zhang, M. Cheng, L. Hu, J. Wan, W. Xiong, M. Wen, X. Wen, L. Qin, Highly porous carbon nitride by supramolecular preassembly of monomers for photocatalytic removal of sulfamethazine under visible light driven, Appl. Catal. B 220 (2018) 202–210, https://doi.org/10.1016/j.apcatb.2017.08.055.